F-box protein FBXW7 inhibits cancer metastasis in a non-cell-autonomous manner

Kanae Yumimoto,[1] Sayuri Akiyoshi,[2] Hiroki Ueo,[2] Yasuaki Sagara,[3] Ichiro Onoyama,[1] Hiroaki Ueo,[4] Shinji Ohno,[5] Masaki Mori,[6] Koshi Mimori,[2] and Keiichi I. Nakayama[1]

[1]Department of Molecular and Cellular Biology, Medical Institute of Bioregulation, Kyushu University, Fukuoka, Japan. [2]Department of Surgery, Kyushu University Beppu Hospital, Beppu, Japan. [3]Sagara Hospital, Kagoshima, Japan. [4]Ueo Breast Surgical Hospital, Oita, Japan. [5]Clinical Research Institute, National Hospital Organization Kyushu Cancer Center, Fukuoka, Japan. [6]Department of Gastroenterological Surgery, Graduate School of Medicine, Osaka University, Suita, Japan.

The gene encoding F-box protein FBXW7 is frequently mutated in many human cancers. Although most previous studies have focused on the tumor-suppressive capacity of FBXW7 in tumor cells themselves, we determined that FBXW7 in the host microenvironment also suppresses cancer metastasis. Deletion of *Fbxw7* in murine BM-derived stromal cells induced accumulation of NOTCH and consequent transcriptional activation of *Ccl2*. FBXW7-deficient mice exhibited increased serum levels of the chemokine CCL2, which resulted in the recruitment of both monocytic myeloid-derived suppressor cells and macrophages, thereby promoting metastatic tumor growth. Administration of a CCL2 receptor antagonist blocked the enhancement of metastasis in FBXW7-deficient mice. Furthermore, in human breast cancer patients, *FBXW7* expression in peripheral blood was associated with serum CCL2 concentration and disease prognosis. Together, these results suggest that FBXW7 antagonizes cancer development in not only a cell-autonomous manner, but also a non-cell-autonomous manner, and that modulation of the FBXW7/NOTCH/CCL2 axis may provide a potential approach to suppression of cancer metastasis.

Introduction

Metastasis is a major cause of death in cancer patients, and elucidation of the genes and mechanisms that underlie this process is expected to provide a basis for the development of new cancer treatments. Such mechanisms have remained poorly understood because of the complexity of metastasis, which includes detachment of cancer cells from a primary tumor followed by their invasion into surrounding tissue, entry into the circulatory system, and invasion and proliferation in distant organs. In addition to the genomic variation among malignant tumor cells, recent research has focused on the relationship between cancer and the host environment. BM-derived cells (BMDCs) — including T cells (1), B cells (2), granulocytic and monocytic myeloid-derived suppressor cells (G-MDSCs and Mo-MDSCs, respectively) (3–6), macrophages (7–10), BM-derived stromal cells (BMSCs) (11, 12), hematopoietic progenitor cells (HPCs) (13), and endothelial progenitor cells (EPCs) (14) — play pivotal roles in promoting metastasis, including facilitation of tumor cell growth and invasion as well as of angiogenesis (15).

Tumor cells and surrounding stromal cells secrete various growth factors, cytokines, and chemokines that promote cancer development (16, 17). Chemokines promote tumor development and progression in addition to recruiting immune cells to tumor sites. The chemokine CCL2 (also known as monocyte chemoattractant protein-1 [MCP-1]) regulates the recruitment of monocytes, macrophages, and other inflammatory cells to sites of inflammation through interaction with its receptor, CCR2 (18). CCL2 also contributes to the recruitment of monocytes/macrophages to sites of pulmonary metastasis in mice with breast cancer and then promotes tumor outgrowth (19). Systemic administration of neutralizing antibodies against CCL2 in mouse cancer models has resulted in marked attenuation of tumor growth, reduction in tumor blood vessel density, and inhibition of metastasis (19–23).

FBXW7 (also known as Fbw7, Sel-10, hCdc4, or hAgo) is the F-box protein component of an Skp1–Cul1–F-box protein–type (SCF-type) ubiquitin ligase, in which it functions as a receptor responsible for substrate recognition. Most of the substrates of FBXW7 are growth promoters, including c-MYC (24, 25), NOTCH (26–28), cyclin E (29–31), c-JUN (32, 33), KLF5 (34, 35), and mTOR (36), and FBXW7 is therefore thought to serve as a tumor suppressor. Analysis of *FBXW7* in many primary human tumors revealed that approximately 6% of the tumors harbored mutations in this gene (37). Mutations were detected most frequently in cholangiocarcinoma (35%) and T cell acute lymphocytic leukemia (T-ALL; 31%). Notably, 43% of the identified mutations were found to be missense mutations that resulted in amino acid substitutions at key arginine residues (Arg^{465} and Arg^{479}) within the WD40 domain that are responsible for substrate recognition, which suggests that defective degradation of FBXW7 substrates leads to tumorigenesis.

Prior findings in genetic analyses of mice in which *Fbxw7* is conditionally deleted in various tissues collectively support a pivotal role for FBXW7 in suppression of tumorigenesis in vivo. Conditional inactivation of *Fbxw7* in the T cell lineage of mice induced the development of thymic lymphoma as a result of excessive c-MYC accumulation (38). More than half of BM-specific FBXW7-deficient mice developed T-ALL within 16 weeks, manifesting

Authorship note: Kanae Yumimoto and Sayuri Akiyoshi contributed equally to this work.
Conflict of interest: The authors have declared that no conflict of interest exists.
Submitted: August 29, 2014; **Accepted:** November 20, 2014.
Reference information: *J Clin Invest.* 2015;125(2):621–635. doi:10.1172/JCI78782.

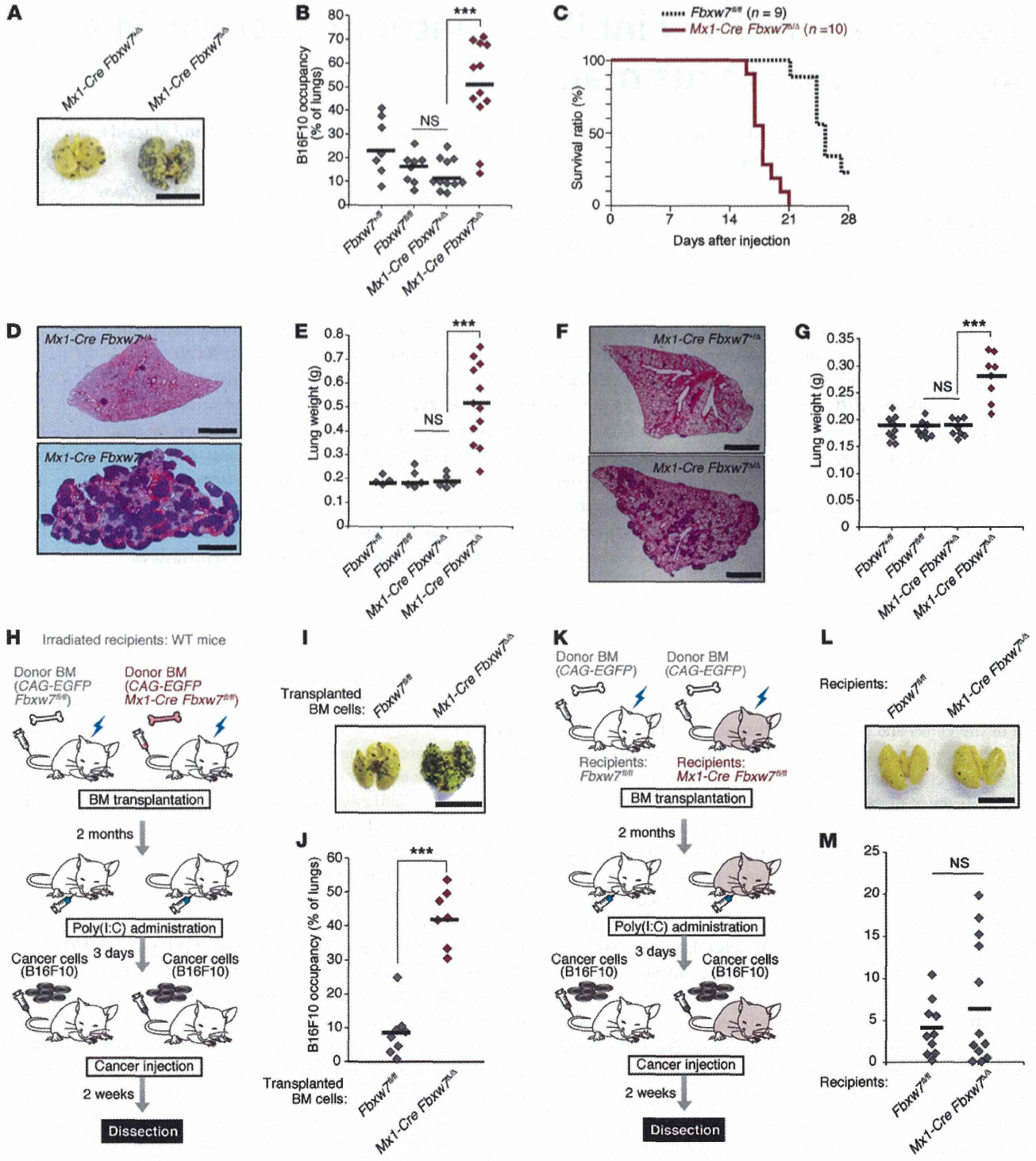

Figure 1. *Fbxw7* deletion in BM promotes cancer metastasis in an intravenous tumor cell transplantation model. (**A** and **B**) B16F10 cells were transplanted into *Fbxw7*$^{+/fl}$ (n = 7), *Fbxw7*$^{fl/fl}$ (n = 8), *Mx1-Cre Fbxw7*$^{+/\Delta}$ (n = 11), and *Mx1-Cre Fbxw7*$^{\Delta/\Delta}$ (n = 12) mice. The gross appearance of the lungs (**A**) and their occupancy by tumor colonies (**B**) were examined. Horizontal bars in **B** indicate mean values. (**C**) Kaplan-Meier survival curves for *Fbxw7*$^{fl/fl}$ (n = 9) and *Mx1-Cre Fbxw7*$^{\Delta/\Delta}$ (n = 10) mice after injection of B16F10 cells. (**D** and **E**) LLC cells were transplanted into *Fbxw7*$^{+/fl}$ (n = 4), *Fbxw7*$^{fl/fl}$ (n = 5), *Mx1-Cre Fbxw7*$^{+/\Delta}$ (n = 5), and *Mx1-Cre Fbxw7*$^{\Delta/\Delta}$ (n = 12) mice. (**F** and **G**) B16F1 cells were transplanted into *Fbxw7*$^{+/fl}$ (n = 9), *Fbxw7*$^{fl/fl}$ (n = 8), *Mx1-Cre Fbxw7*$^{+/\Delta}$ (n = 8), and *Mx1-Cre Fbxw7*$^{\Delta/\Delta}$ (n = 8) mice. Lungs were subjected to H&E staining (**D** and **F**), and their gross weight was determined (**E** and **G**). (**H**–**J**) Metastasis assays performed in WT mice reconstituted with *CAG-EGFP Fbxw7*$^{fl/fl}$ (n = 8) or *CAG-EGFP Mx1-Cre Fbxw7*$^{\Delta/\Delta}$ (n = 7) donor BM. (**K**–**M**) Metastasis assays performed in *Fbxw7*$^{fl/fl}$ (n = 10) or *Mx1-Cre Fbxw7*$^{\Delta/\Delta}$ (n = 12) mice reconstituted with WT donor BM. Schematic representation (**H** and **K**), gross appearance of the lungs (**I** and **L**), and their occupancy by tumor colonies (**J** and **M**) are shown. Scale bars: 10 mm (**A**, **I**, and **L**); 2 mm (**D** and **F**). Horizontal bars in **B**, **E**, **G**, **J**, and **M** indicate means. ***$P < 0.001$, 1-way ANOVA and Bonferroni test (**B**, **E**, and **G**) or 2-tailed Student's t test (**J**).

marked accumulation of NOTCH1 and c-MYC proteins (39, 40). FBXW7-null mice harboring a mutation in the adenomatous polyposis coli (*Apc*) gene (*Fbxw7*$^{\Delta/\Delta}$ *Apc*$^{min/+}$ mice) showed an increase in both number and size of intestinal tumors, and a consequently reduced survival rate, compared with *Apc*$^{min/+}$ mice (41). These various observations thus suggest that FBXW7 is a potent tumor suppressor in mice as well as in humans.

In the present study, we show that FBXW7 expression in the host environment is a key determinant of cancer metastasis. Metastasis was found to be enhanced in mice lacking FBXW7 in BM compared with control mice. We characterized the mechanism underlying this enhancement of metastasis: deletion of *Fbxw7* resulted in NOTCH accumulation and consequent activation of *Ccl2* gene transcription in BMSCs. The increased production of CCL2 by these cells likely promoted the formation of metastatic niches through recruitment of Mo-MDSC and macrophages. Inhibition of CCL2/CCR2 signaling reduced the frequency of metastasis in the FBXW7-deficient mice. Our results thus suggest that the FBXW7/NOTCH/CCL2 pathway plays a central role in the regulation of cancer metastasis.

Results

Deletion of Fbxw7 in BM promotes cancer metastasis in mice. Most studies of FBXW7 have focused on its functions in tumor cells (42–44); little is known regarding the role of this protein in the host microenvironment with respect to tumor development. To investigate the role of FBXW7 in the host microenvironment, we transferred B16F10 melanoma cells into the tail vein of *Mx1-Cre Fbxw7*$^{fl/fl}$ mice that had been injected with polyinosinic:polycytidylic acid [poly(I:C)] to delete floxed *Fbxw7* alleles selectively in BM (referred to hereafter as *Mx1-Cre Fbxw7*$^{\Delta/\Delta}$ mice). The frequency of metastasis of the melanoma cells to the lungs was markedly increased in *Mx1-Cre Fbxw7*$^{\Delta/\Delta}$ versus control mice (Figure 1, A and B), and this increased metastasis was accompanied by earlier death of the *Mx1-Cre Fbxw7*$^{\Delta/\Delta}$ mice (Figure 1C). Similar results were obtained when Lewis lung carcinoma (LLC) cells (Figure 1, D and E, and Supplemental Figure 1, A–C; supplemental material available online with this article; doi:10.1172/JCI78782DS1) or low-metastatic potential B16F1 melanoma cells (Figure 1, F and G, and Supplemental Figure 1, D–F) were injected into the tail vein of these mice. Thus, the level of FBXW7 in BM represents a key determinant of cancer metastasis in mice.

To examine whether ablation of *Fbxw7* specifically in BM was indeed responsible for the enhanced metastasis in *Mx1-Cre Fbxw7*$^{\Delta/\Delta}$ mice, we transplanted BM cells from *Mx1-Cre Fbxw7*$^{fl/fl}$ or control *Fbxw7*$^{fl/fl}$ mice that also harbor a transgene for enhanced green fluorescent protein (*EGFP*) under the control of the *CAG* promoter into irradiated C57BL/6 mice (Figure 1H). The recipient mice were subsequently injected with poly(I:C) to delete floxed alleles of *Fbxw7*; 3 days after injection, B16F10 or LLC cancer cells were transferred to these mice. Metastasis to the lungs was more pronounced in mice receiving *CAG-EGFP Mx1-Cre Fbxw7*$^{fl/fl}$ BM cells than in those receiving the control cells (Figure 1, I and J, and Supplemental Figure 1, G and H). In contrast, a reciprocal experiment revealed no such enhancement of metastasis in *Mx1-Cre Fbxw7*$^{fl/fl}$ mice subjected to transplantation with BM from *CAG-EGFP* mice and injected with poly(I:C) (Figure 1, K–M). These results confirmed that the loss of FBXW7 in BM is indeed responsible for the increased frequency of metastasis observed in *Mx1-Cre Fbxw7*$^{\Delta/\Delta}$ mice.

We also examined metastatic tumor growth in control and *Mx1-Cre Fbxw7*$^{\Delta/\Delta}$ mice after orthotopic transplantation of E0771 mouse breast cancer cells. Primary tumor growth was promoted in FBXW7-deficient mice on days 17 and 20, albeit not at later time points (Figure 2, A and B). Metastasis to the lungs was markedly enhanced in the mutant mice (Figure 2, C and D). In addition to lung weight, the total tumor area, number of tumor nodules, and average area per nodule in the lungs were greater for *Mx1-Cre Fbxw7*$^{\Delta/\Delta}$ mice than controls (Figure 2, D–G). We next monitored the progression of metastatic tumors in this model. Whereas we did not detect any tumor cells in the lungs at 12 days after cell transplantation, metastasis of E0771 cells was apparent in both control and *Mx1-Cre Fbxw7*$^{\Delta/\Delta}$ mice at 16 days (Figure 2, H–J). The number of tumor nodules and the average area per nodule did not differ between genotypes at 16 days after transplantation, but were significantly greater in *Mx1-Cre Fbxw7*$^{\Delta/\Delta}$ mice than in controls at 20 days. Although a premetastatic niche was previously shown to be formed by clusters of BMDCs (13), we found that such EGFP$^+$ clusters were already present at day 0 (before E0771 cell transplantation) in the lungs of WT mice reconstituted with EGFP-labeled *Mx1-Cre Fbxw7*$^{\Delta/\Delta}$ or control BM cells (Supplemental Figure 2A). The number of these clusters did not change substantially with time after E0771 cell transplantation and did not differ between the genotypes (Supplemental Figure 2B). In contrast, the number of diffusely infiltrated BMDCs in the lungs was increased after tumor cell transplantation specifically in mice reconstituted with *Mx1-Cre Fbxw7*$^{\Delta/\Delta}$ BM cells (Supplemental Figure 2, A and C). Immunofluorescence analysis with antibodies against TCRβ (for T cells), B220 (for B cells), Ly6G (for G-MDSCs), Ly6C (for Mo-MDSCs), F4/80 (for monocytes/macrophages), fibroblast-specific protein (FSP; for stromal cells), MAC1 (for myeloid cells), c-KIT (for HPCs), and VE-cadherin (for EPCs) revealed that the number of Ly6C$^+$, F4/80$^+$, and MAC1$^+$ cells increased among tumor-surrounding BMDCs, whereas only B220$^+$ cells moderately increased in number among the nonsurrounding BMDCs (Figure 3, A–F, and Supplemental Figure 3, A–C). These results suggested that accumulation of Mo-MDSCs or of more differentiated macrophages might be responsible for the promotion of metastasis in *Mx1-Cre Fbxw7*$^{\Delta/\Delta}$ mice.

We also characterized cells in the peripheral blood of mice at various times from 2 days before to 32 days after tumor cell transplantation. The frequency of MAC1$^+$Ly6G$^-$Ly6C$^+$ Mo-MDSCs and MAC1$^+$F4/80$^+$CD115$^+$ monocytes/macrophages in peripheral blood increased in *Mx1-Cre Fbxw7*$^{\Delta/\Delta}$ versus control mice before tumor cell transplantation, whereas the frequency of MAC1$^+$Ly6G$^+$Ly6C$^+$ immature MDSCs did not differ between the genotypes at this time (Supplemental Figure 2, D–F). However, the frequency of these latter cells in peripheral blood increased transiently — to a greater extent in *Mx1-Cre Fbxw7*$^{\Delta/\Delta}$ mice than in control mice — between days 16 and 24. In contrast, the frequency of MAC1$^+$Ly6G$^-$Ly6C$^+$ Mo-MDSCs in BM did not differ between genotypes at day 0 or day 20 (Supplemental Figure 2, G and H). Collectively, these results suggested that the increased infiltration of BMDCs during the early phase of metastasis to the lungs in *Mx1-Cre Fbxw7*$^{\Delta/\Delta}$ mice might rep-

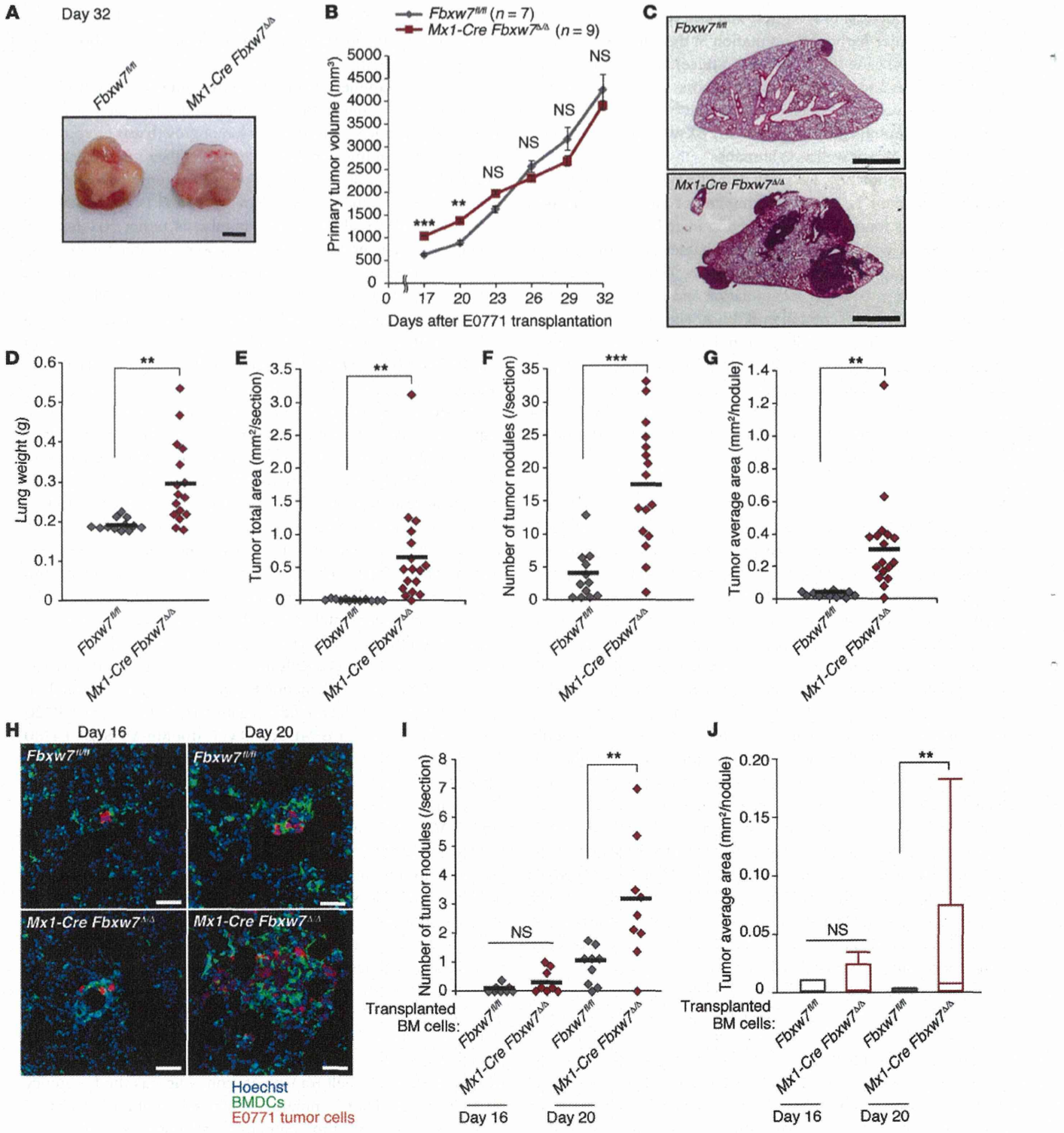

Figure 2. *Fbxw7* deletion in BM promotes cancer metastasis in an orthotopic breast cancer transplantation model. (**A** and **B**) E0771 cells were transplanted into the mammary fat pad of *Fbxw7*$^{fl/fl}$ (n = 11) and *Mx1-Cre Fbxw7*$^{Δ/Δ}$ (n = 13) mice. Primary tumor gross appearance after 32 days (**A**) and volume at the indicated times (**B**) are shown. (**C**–**G**) E0771 cells were transplanted into the mammary fat pad of *Fbxw7*$^{fl/fl}$ (n = 12) and *Mx1-Cre Fbxw7*$^{Δ/Δ}$ (n = 16) mice. After 32 days, lungs were subjected to H&E staining (**C**), and their gross weight was determined (**D**). Tumor total area (**E**), number of tumor nodules (**F**), and average tumor area (**G**) were calculated from the stained lung sections. (**H**–**J**) WT mice were reconstituted with BM cells of the indicated mice and subjected to orthotopic transplantation with tdTomato-labeled E0771 cells. Lungs were subjected to fluorescence microscopy for detection of BMDCs (green), tumor cells (red), and cell nuclei (Hoechst 33238) (**H**), and the number of tumor nodules (**I**) and average tumor area (**J**) were determined 16 (n = 8 per group) or 20 (n = 9 per group) days after tumor cell transplantation. Scale bars: 2 mm (**C**); 100 μm (**H**). Data in **B** are mean ± SEM; horizontal bars in **D**–**G** and **I** indicate means; box and whisker plots in **J** depict the smallest value, lower quartile, median, upper quartile, and largest value. $^{**}P < 0.01$, $^{***}P < 0.001$, 2-tailed Student's t test (**B**, **D**–**G**, **I**, and **J**).

resent increased migration or recruitment of Mo-MDSCs and macrophages, rather than differentiation of these cells in BM.

Serum chemokine levels are increased in mice lacking FBXW7 in BM. To explore the mechanism responsible for this increased mobilization of Mo-MDSCs and macrophages induced by FBXW7 deficiency, we examined the serum concentrations of various cytokines before and after E0771 cell transplantation. Cytokine array analysis revealed that the levels of CCL2, CCL12 (also known as MCP-5), and the chemokine CXCL13 (also known as B lymphocyte chemoattractant [BLC]) were increased more than 2-fold in *Mx1-Cre Fbxw7*$^{\Delta/\Delta}$ versus control mice both before and after E0771 cell transplantation (Figure 4A and Supplemental Figure 4). Both CCL2 and CCL12 induce the migration of monocytes/macrophages by binding to their common receptor, CCR2. CCL12 is mainly secreted from macrophages, but *Fbxw7* ablation in the macrophages of *LysM-Cre Fbxw7*$^{fl/fl}$ mice did not affect metastasis frequency (Supplemental Figure 5, A and B), which suggests that CCL12 is not largely responsible for the promotion of metastasis. We thus focused on CCL2 and found greater serum CCL2 concentrations in *Mx1-Cre Fbxw7*$^{\Delta/\Delta}$ mice compared with control mice both before and after E0771 cell transplantation (Figure 4B).

To examine whether the enhanced metastasis apparent in FBXW7-deficient mice is dependent on the CCL2/CCR2 pathway, we treated *Mx1-Cre Fbxw7*$^{\Delta/\Delta}$ mice with propagermanium, a CCR2 antagonist. The extent of B16F10 or E0771 cell metastasis in *Mx1-Cre Fbxw7*$^{\Delta/\Delta}$ mice was significantly attenuated by propagermanium administration (Figure 4, C–H). The frequency of EGFP$^+$Ly6C$^+$ cells in the lungs of WT mice reconstituted with EGFP-labeled *Mx1-Cre Fbxw7*$^{\Delta/\Delta}$ BM cells and injected with E0771 cells was also significantly reduced by propagermanium treatment (Figure 4H). Unexpectedly, the number of tumor nodules in the lungs was not affected by propagermanium treatment, whereas the size of each nodule was markedly reduced in the treated mice (Figure 4, F and G). Collectively, these results suggested that the increased production of CCL2 by FBXW7-deficient BMDCs promotes the growth of tumors that have already metastasized to the lungs.

The Ccl2 gene is activated in FBXW7-deficient BMSCs. We next investigated which cells of the BM are responsible for the metastasis promotion and increased serum CCL2 concentration observed in FBXW7-deficient mice. For these experiments, we used mice deficient in FBXW7 in different lineages. *LysM-Cre Fbxw7*$^{-/\Delta}$ mice, in which the *Cre* gene is activated to delete floxed *Fbxw7* alleles only in the granulocyte-macrophage lineage, did not show an increase in metastasis frequency compared with control mice (Supplemental Figure 5, A and B). Furthermore, neither *Lck-Cre Fbxw7*$^{\Delta/\Delta}$ nor *Cd19-Cre Fbxw7*$^{\Delta/\Delta}$ mice (*Fbxw7* deletion specific to T and B cells, respectively) showed enhancement of metastasis like that in *Mx1-Cre Fbxw7*$^{\Delta/\Delta}$ mice (Supplemental Figure 5, C–F). These results suggested that neither myeloid (granulocyte and macrophage) nor lymphoid (T and B cell) lineages are responsible for the promotion of metastasis induced by BM *Fbxw7* ablation.

Neither the serum level of CCL2 nor the frequency of MAC1$^+$F4/80$^+$ monocytes/macrophages in peripheral blood differed between *LysM-Cre Fbxw7*$^{-/\Delta}$ and control mice (Supplemental Figure 6, A and B), which suggests that monocytes/macrophages are not the major source of CCL2 produced in response to *Fbxw7* loss. We found that FSP$^+$ BMSCs colocalized with metastatic tumor cells and Mo-MDSCs in the lungs of mice after orthotopic transplantation of E0771 cells (Figure 5A). Given that BMSCs were previously shown to secrete CCL2 and to contribute to the emigration of monocytes from BM (45, 46), we hypothesized that BMSCs might be a major source of CCL2 production in our models. To test this hypothesis, we isolated BMSCs from BM of *CAG-Cre-ER*^{T2} *Fbxw7*$^{fl/fl}$ (or control *Fbxw7*$^{fl/fl}$) mice and treated them with 10 μM tamoxifen to induce deletion of floxed *Fbxw7* alleles (Figure 5B). The abundance of *Ccl2* mRNA was increased in *CAG-Cre-ER*^{T2} *Fbxw7*$^{\Delta/\Delta}$ BMSCs compared with control cells (Figure 5C). The amount of CCL2 released from *CAG-Cre-ER*^{T2} *Fbxw7*$^{\Delta/\Delta}$ BMSCs into the culture medium was also substantially greater than that released from control cells (Figure 5D). Furthermore, the introduction of WT *Fbxw7a* cDNA into *CAG-Cre-ER*^{T2} *Fbxw7*$^{\Delta/\Delta}$ BMSCs resulted in a marked decrease in the abundance of *Ccl2* mRNA, whereas introduction of cDNA for a mutant form of *Fbxw7a* that lacks the F-box domain (ΔF) had no such effect (Figure 5E), which suggests that FBXW7 negatively regulates CCL2 production in BMSCs.

To examine whether the increased CCL2 production by BMSCs is responsible for the promotion of cancer metastasis in FBXW7-deficient mice, we depleted *CAG-Cre-ER*^{T2} *Fbxw7*$^{\Delta/\Delta}$ BMSCs of CCL2 by shRNA-mediated RNAi (Figure 5F) and then transferred these cells, together with B16F10 melanoma cells, into recipient mice via the tail vein. BMSCs were detected in many tissues, such as BM and lungs, even 4 months after transplantation (47). The extent of lung metastasis in recipient mice was increased by *Fbxw7*$^{\Delta/\Delta}$ versus control BMSCs when coinjected with melanoma cells (Figure 5, G and H). However, this effect of *Fbxw7* deletion was abolished by depletion of CCL2 in BMSCs, which suggests that the increased production of CCL2 by FBXW7-deficient BMSCs contributes to the promotion of metastasis.

NOTCH accumulation in FBXW7-deficient BMSCs promotes metastasis by increasing CCL2 production. Immunoblot analysis revealed that, among the FBXW7 substrates examined, NOTCH1 intracellular domain (NICD1), c-MYC, and KLF5 accumulated at high levels in FBXW7-deficient BMSCs (Figure 6A). Forced expression of NICD1 in WT BMSCs resulted in a marked increase both in the abundance of *Ccl2* mRNA and in the activity of the *Ccl2* gene promoter, whereas that of c-MYC or KLF5 had no such effects (Figure 6, B and C). Inhibition of NOTCH signaling in FBXW7-deficient BMSCs by exposure to the γ-secretase inhibitor *N*-[*N*-(3,5-difluorophenacetyl)-L-alanyl]-*S*-phenylglycine *t*-butyl ester (DAPT) resulted in a concentration-dependent reduction in the amount of *Ccl2* mRNA (Figure 6D). The promoter of the mouse *Ccl2* gene contains 4 consensus sequences for NOTCH binding (Figure 6E and ref. 48), and a luciferase reporter assay with WT and mutant forms of this promoter indicated that the first 2 upstream elements are required for full promoter activity (Figure 6F). This finding was consistent with the results of ChIP analysis showing that NICD1 was associated with the distal region of the *Ccl2* gene promoter in *Fbxw7*$^{\Delta/\Delta}$ BMSCs (Figure 6G). Together, these observations suggested that the NOTCH/CCL2 pathway in BMSCs contributes to the promotion of metastasis in FBXW7-deficient mice.

We further evaluated this notion by genetic analyses. Additional ablation of RBP-Jκ, an essential cofactor for NOTCH-dependent transactivation, markedly attenuated the enhanced metastasis observed in *Mx1-Cre Fbxw7*$^{\Delta/\Delta}$ mice (Figure 6, H and I).

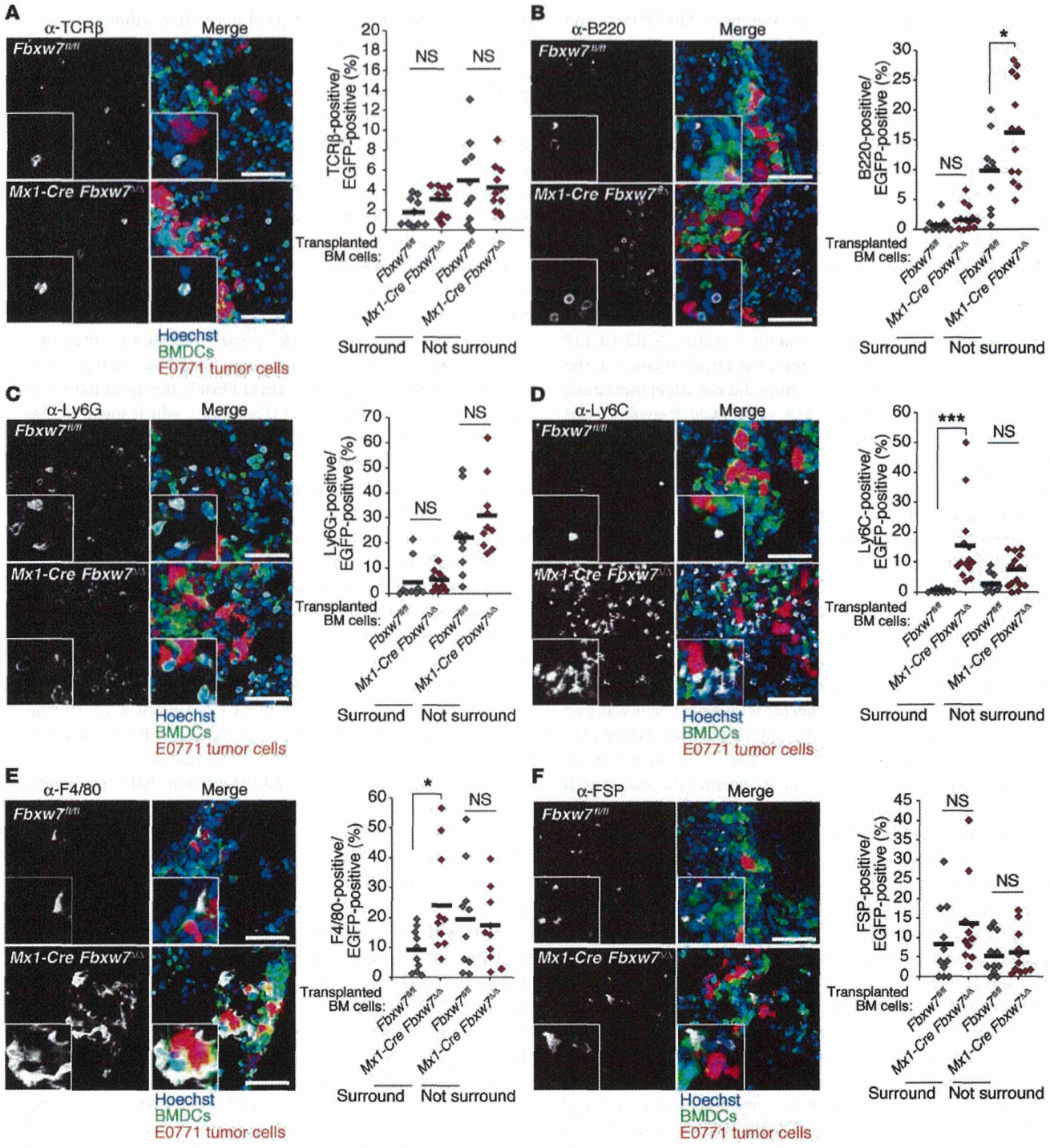

Figure 3. Ly6C⁺ Mo-MDSCs and F4/80⁺ monocytes/macrophages accumulate in the microenvironment of metastatic tumors in the lungs of mice reconstituted with FBXW7-deficient BM cells. Representative immunohistofluorescence staining (white) for TCRβ (**A**), B220 (**B**), Ly6G (**C**), Ly6C (**D**), F4/80 (**E**), and FSP (**F**) for lung sections from WT mice reconstituted with *CAG-EGFP Fbxw7*$^{fl/fl}$ (n = 10 [**A**, **B**, **D**, and **E**]; 9 [**C**]; 11 [**F**]) or *CAG-EGFP Mx1-Cre Fbxw7*$^{\Delta/\Delta}$ (n = 10 [**A**, **C**, and **E**]; 12 [**B**]; 14 [**D**]; 11 [**F**]) BM cells and subjected to orthotopic transplantation with tdTomato-labeled E0771 cells (20 days before analysis) as in Figure 2H. Intrinsic fluorescence of EGFP (green), tdTomato (red), and Hoechst 33258 (blue) was also imaged. Higher-magnification images (×2) are shown in the insets. Scale bars: 100 μm. The percentage of EGFP⁺ BMDCs positive for each marker in tumor-surrounding and nonsurrounding regions was quantified; horizontal bars indicate means. $^*P < 0.05$, $^{***}P < 0.001$, 1-way ANOVA and Bonferroni test.

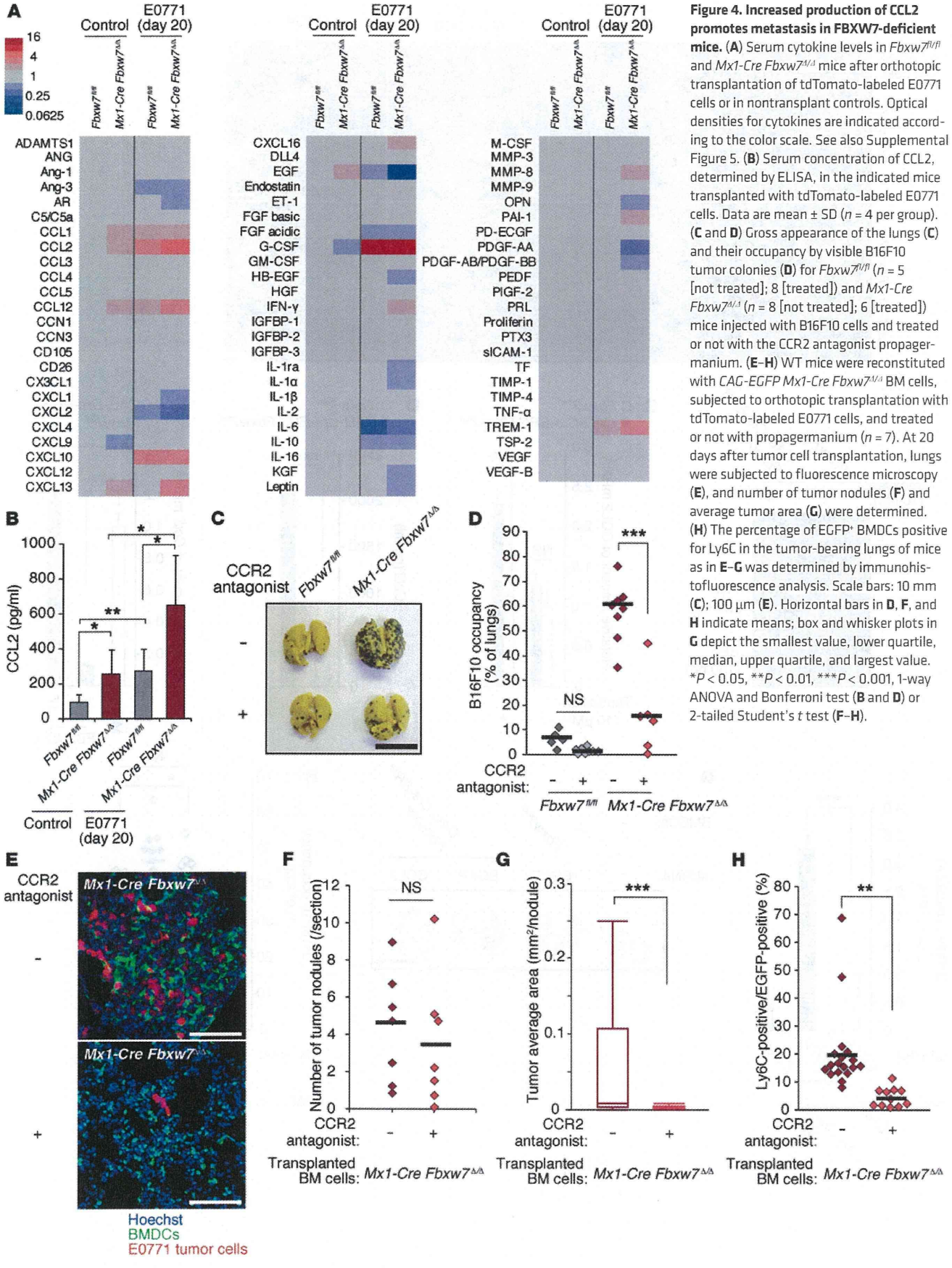

Figure 4. Increased production of CCL2 promotes metastasis in FBXW7-deficient mice. (**A**) Serum cytokine levels in *Fbxw7*$^{fl/fl}$ and *Mx1-Cre Fbxw7*$^{Δ/Δ}$ mice after orthotopic transplantation of tdTomato-labeled E0771 cells or in nontransplant controls. Optical densities for cytokines are indicated according to the color scale. See also Supplemental Figure 5. (**B**) Serum concentration of CCL2, determined by ELISA, in the indicated mice transplanted with tdTomato-labeled E0771 cells. Data are mean ± SD (n = 4 per group). (**C** and **D**) Gross appearance of the lungs (**C**) and their occupancy by visible B16F10 tumor colonies (**D**) for *Fbxw7*$^{fl/fl}$ (n = 5 [not treated]; 8 [treated]) and *Mx1-Cre Fbxw7*$^{Δ/Δ}$ (n = 8 [not treated]; 6 [treated]) mice injected with B16F10 cells and treated or not with the CCR2 antagonist propagermanium. (**E**–**H**) WT mice were reconstituted with *CAG-EGFP Mx1-Cre Fbxw7*$^{Δ/Δ}$ BM cells, subjected to orthotopic transplantation with tdTomato-labeled E0771 cells, and treated or not with propagermanium (n = 7). At 20 days after tumor cell transplantation, lungs were subjected to fluorescence microscopy (**E**), and number of tumor nodules (**F**) and average tumor area (**G**) were determined. (**H**) The percentage of EGFP$^+$ BMDCs positive for Ly6C in the tumor-bearing lungs of mice as in **E**–**G** was determined by immunohistofluorescence analysis. Scale bars: 10 mm (**C**); 100 μm (**E**). Horizontal bars in **D**, **F**, and **H** indicate means; box and whisker plots in **G** depict the smallest value, lower quartile, median, upper quartile, and largest value. $^*P < 0.05$, $^{**}P < 0.01$, $^{***}P < 0.001$, 1-way ANOVA and Bonferroni test (**B** and **D**) or 2-tailed Student's t test (**F**–**H**).

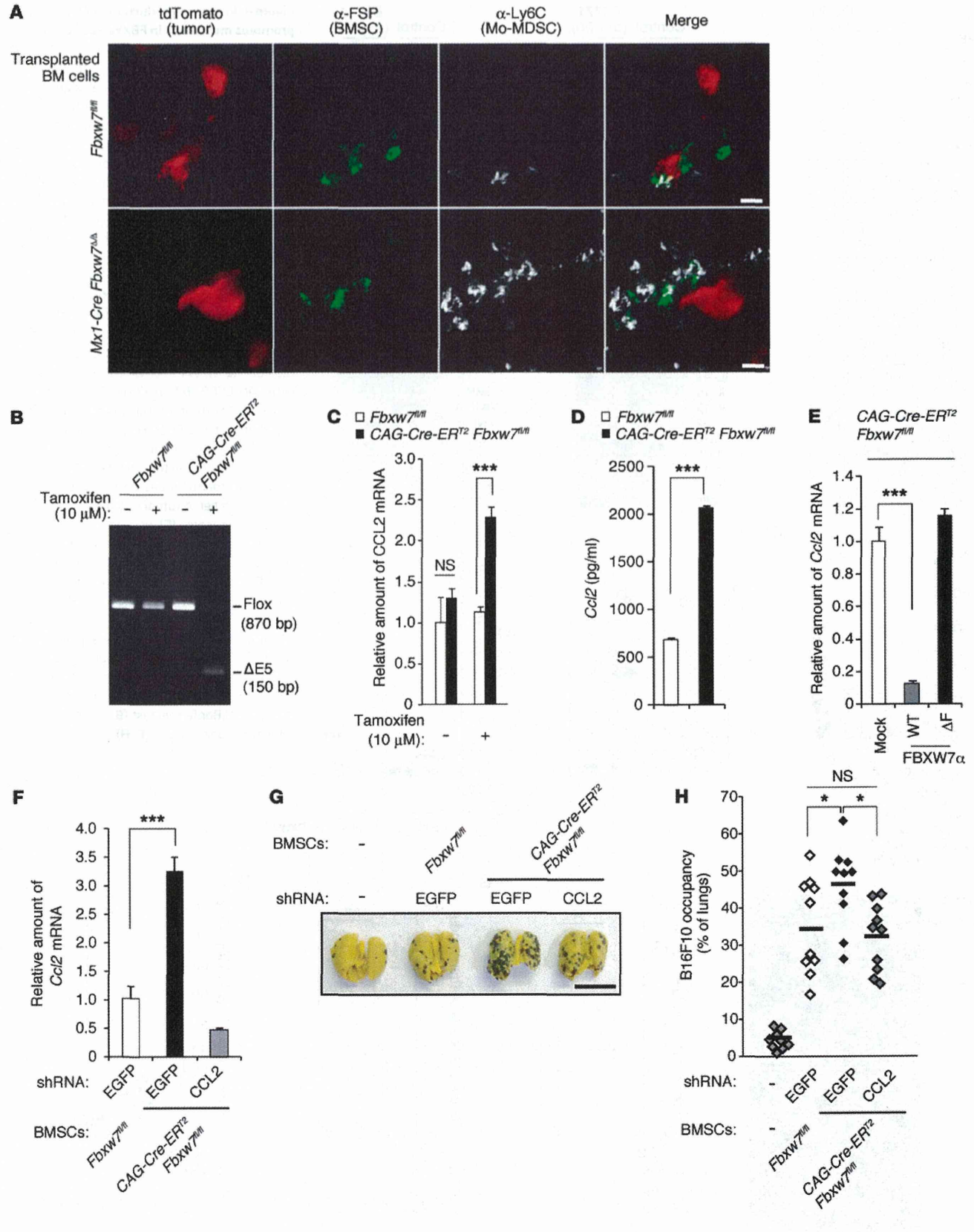

Figure 5. Increased *Ccl2* gene expression in FBXW7-deficient BMSCs promotes cancer metastasis. (**A**) Representative immunohistofluorescence staining of Ly6C and FSP in lung sections from WT mice reconstituted with indicated BM cells and subjected to orthotopic transplantation with tdTomato-labeled E0771 cells (20 days before analysis). (**B**) Genomic PCR analysis of BMSCs from the indicated mice incubated in the absence or presence of 10 μM tamoxifen. The positions of amplified fragments corresponding to floxed and exon 5–deleted (ΔE5) *Fbxw7* alleles are indicated. (**C**) Relative abundance of *Ccl2* mRNA in BMSCs from the indicated mice. (**D**) Concentration of CCL2 released into culture supernatants from the indicated BMSCs. (**E**) Relative abundance of *Ccl2* mRNA in *CAG-Cre-ER*^{T2} *Fbxw7*$^{\Delta/\Delta}$ BMSCs infected with retroviruses encoding WT or ΔF mutant forms of FBXW7α or with the empty virus (Mock). (**F**) Relative abundance of *Ccl2* mRNA in BMSCs from *Fbxw7*$^{fl/fl}$ or *CAG-Cre-ER*^{T2} *Fbxw7*$^{fl/fl}$ mice treated with tamoxifen and subjected to RNAi with shRNA vectors targeting EGFP (control) or CCL2. (**G** and **H**) Gross appearance of the lungs (**G**) and their occupancy by visible B16F10 colonies (**H**) for WT mice 2 weeks after injection both with B16F10 cells and with BMSCs isolated from the indicated mice and treated as in **F** (n = 10 per group). Scale bars: 10 μm (**A**), 10 mm (**G**). Data are mean ± SD (**C**–**F**); horizontal bars in **H** indicate means. $^*P < 0.05$, $^{***}P < 0.001$, 1-way ANOVA and Bonferroni test (**C**, **E**, **F**, and **H**) or 2-tailed Student's t test (**D**).

In contrast, inactivation of c-MYC in *Mx1-Cre Fbxw7*$^{\Delta/\Delta}$ mice had no such effect (Figure 6, J and K). Additional ablation of RBP-Jκ, but not that of c-MYC, also reduced the serum concentration of CCL2 to the control level in *Mx1-Cre Fbxw7*$^{\Delta/\Delta}$ mice (Figure 6L).

Low FBXW7 expression in the host microenvironment is associated with poor prognosis in breast cancer patients. To extend our observations in mice to humans, we measured the abundance of *FBXW7* mRNA in peripheral blood of breast cancer specimens and examined the relationship between *FBXW7* mRNA abundance and prognosis. The prognosis of individuals with low *FBXW7* expression in peripheral blood was significantly poorer than that of those in the corresponding high-*FBXW7* group (Figure 7, A and B), consistent with our model. The difference in prognosis between the low- and high-expression groups was even more pronounced when the analysis was restricted to patients with tumors triple-negative for estrogen receptor (ER), progesterone receptor (PR), and HER2 (Figure 7, C–E) or to those with tumors of high histological grade or low stage (Supplemental Figure 7, A–G). The frequency of CD45$^-$ circulating tumor cells that expressed CD326 (also known as EpCAM) was at most 0.003% of total blood mononuclear cells (Supplemental Figure 7H), which suggests that the contribution of such cells to the total abundance of *FBXW7* mRNA in peripheral blood is negligible.

Immunohistochemical analysis of FBXW7 in primary tumor lesions revealed that the abundance of *FBXW7* mRNA in peripheral blood was not significantly correlated with FBXW7 expression in tumor cells, but was highly correlated with that in surrounding stromal cells (Figure 7, F–H). These results suggested that the abundance of *FBXW7* mRNA in peripheral blood is a marker for FBXW7 expression in stromal cells that surround tumor cells. We also observed a negative correlation between *FBXW7* mRNA abundance in peripheral blood and serum CCL2 concentration (Figure 7I). High serum levels of CCL2 were associated with poor prognosis in breast cancer patients (S. Akiyoshi and K. Mimori, unpublished observation). These data support our concept that FBXW7 ablation gives rise to increased CCL2 production, facilitating metastatic tumor growth (Figure 8).

Discussion

The *FBXW7* gene is a potent tumor suppressor, as evidenced by the many corresponding mutations associated with human cancer (37) as well as by the tumor formation observed in conditional knockout mice (38, 39, 41). The anticancer function of FBXW7 is thought to be mediated by specific ubiquitylation both of growth-promoting oncoproteins — such as c-MYC (24, 25), NOTCH (26, 27, 49), cyclin E (29–31), c-JUN (32, 33), KLF5 (34, 35), and mTOR (36) — and of the antiapoptotic molecule MCL-1 (50, 51). Most previous studies have focused on the tumor-suppressive role of FBXW7 in tumor cells themselves. The putative tumor suppressor C/EBPδ was shown to inhibit FBXW7 expression and to promote mammary tumor metastasis through attenuation of FBXW7-dependent degradation of mTOR in tumor cells (52). We have now discovered what we believe to be a new aspect of FBXW7 function in tumor suppression — namely, its role in the host environment to suppress cancer metastasis. Our data also provide mechanistic insight into the suppression of cancer metastasis by FBXW7. We found that NOTCH, one of the major substrates of FBXW7, activated transcription of the gene encoding CCL2, one of the most well-characterized chemokines with respect to cancer development. Our human clinical data, showing that reduced *FBXW7* expression in peripheral blood was associated with a poor prognosis in breast cancer patients, appeared to be consistent with our experimental results in mice. We therefore propose that the FBXW7/NOTCH/CCL2 axis in the host environment limits cancer metastasis.

CCL2 is thought to be secreted from both cancer cells and noncancer cells in the tumor environment. In a xenograft model in which human cancer cells were transplanted into mice, administration of antibodies specific for human or mouse CCL2 inhibited tumor growth and metastasis, which supports the notion that CCL2 secreted from both the tumor and the host environment plays a key role in tumor development (19, 21). It is likely that the FBXW7/NOTCH1/CCL2 axis in cancer cells also plays a key role in metastasis. We showed here that the level of *FBXW7* expression in peripheral blood was related to prognosis in breast cancer patients. These results thus suggest that constitutional variability in *FBXW7* expression might be an important determinant of prognosis. We propose that the level of *FBXW7* expression is a potentially powerful prognostic marker for cancer patients in general, and that targeting the CCL2/CCR2 system might prove a rational approach for preventing cancer metastasis. Indeed, we found that the CCR2 antagonist propagermanium had a marked inhibitory effect on cancer metastasis in mice. Propagermanium is currently administered clinically for the treatment of individuals with hepatitis B virus infection, and its long-term safety has been well demonstrated. Our results suggest that evaluation of this drug for its ability to inhibit cancer metastasis in humans is warranted.

We found that the number of tumor nodules in the lungs and the average area per nodule were greater in FBXW7-deficient mice than in controls subjected to orthotopic transplantation of breast cancer cells. Unexpectedly, however, treatment with propagermanium did not affect the number of tumor nodules, although the size of each nodule and the frequency of associated Mo-MDSCs were markedly reduced. Collectively, these results suggest that CCL2-dependent infiltration of Mo-MDSCs in the lungs influences the growth of established metastatic tumors rather than the